



**HAL**  
open science

## A meta-analysis of the mechanical properties of ice-templated ceramics and metals

Sylvain Deville, Sylvain Meille, Jordi Seuba,

► **To cite this version:**

Sylvain Deville, Sylvain Meille, Jordi Seuba,. A meta-analysis of the mechanical properties of ice-templated ceramics and metals. *Science and Technology of Advanced Materials*, 2015, 16 (4), pp.043501. 10.1088/1468-6996/16/4/043501 . hal-01273542

**HAL Id: hal-01273542**

**<https://hal.science/hal-01273542>**

Submitted on 16 May 2018

**HAL** is a multi-disciplinary open access archive for the deposit and dissemination of scientific research documents, whether they are published or not. The documents may come from teaching and research institutions in France or abroad, or from public or private research centers.

L'archive ouverte pluridisciplinaire **HAL**, est destinée au dépôt et à la diffusion de documents scientifiques de niveau recherche, publiés ou non, émanant des établissements d'enseignement et de recherche français ou étrangers, des laboratoires publics ou privés.

## Review

# A meta-analysis of the mechanical properties of ice-templated ceramics and metals

Sylvain Deville<sup>1</sup>, Sylvain Meille<sup>2</sup> and Jordi Seuba<sup>1</sup><sup>1</sup>Laboratoire de Synthèse et Fonctionnalisation des Céramiques, UMR3080 CNRS/Saint-Gobain, F-84306 Cavaillon, France<sup>2</sup>Université de Lyon, INSA-Lyon, MATEIS CNRS UMR5510, F-69621 Villeurbanne, FranceE-mail: [sylvain.deville@saint-gobain.com](mailto:sylvain.deville@saint-gobain.com)

Received 6 March 2015, revised 9 June 2015

Accepted for publication 10 June 2015

Published 16 July 2015



CrossMark

**Abstract**

Ice templating, also known as freeze casting, is a popular shaping route for macroporous materials. Over the past 15 years, it has been widely applied to various classes of materials, and in particular ceramics. Many formulation and process parameters, often interdependent, affect the outcome. It is thus difficult to understand the various relationships between these parameters from isolated studies where only a few of these parameters have been investigated. We report here the results of a meta analysis of the structural and mechanical properties of ice templated materials from an exhaustive collection of records. We use these results to identify which parameters are the most critical to control the structure and properties, and to derive guidelines for optimizing the mechanical response of ice templated materials. We hope these results will be a helpful guide to anyone interested in such materials.

Keywords: ceramics, crystal growth, mechanical properties, porous materials

**1. Introduction**


Ice templating, or freeze casting [1], has become a popular shaping route for all kinds of macroporous materials. The process is based on the segregation of matter (particles or solute) by growing crystals in a suspension or solution (figure 1). After complete solidification, the solvent crystals are removed by sublimation. The porosity obtained is thus an almost direct replica of the solvent crystals.

Over the past 15 years, ice templating has been applied to all classes of materials, especially ceramics. Although a few review papers [1–6] have been published, they mostly focus

on the underlying principles. Little can be found on the range of properties that could be achieved.

Ice templating is a complex process, where many parameters can affect the results: formulation of the suspension (nature of the solvent, particle size of the starting powder, solid loading, binder, surfactant, nature of the material, pH, viscosity), freezing conditions (setup, temperature, cooling rate), and measurements conditions (sample dimensions, loading rate, setup). Every article within the scientific literature provides a set of these parameters. The influence of only a few of these parameters has been systematically investigated. The complex interdependent relationships of these parameters cannot be captured in a single, isolated paper.

The many names used for this process hinder a literature review. Throughout the paper, we refer to the process as *ice templating*, probably the most popular term, albeit not the most appropriate. Ice templating implies that water is used. A variety of solvents have been used to date: water [8],

 Content from this work may be used under the terms of the [Creative Commons Attribution 3.0 licence](https://creativecommons.org/licenses/by/3.0/). Any further distribution of this work must maintain attribution to the author(s) and the title of the work, journal citation and DOI.

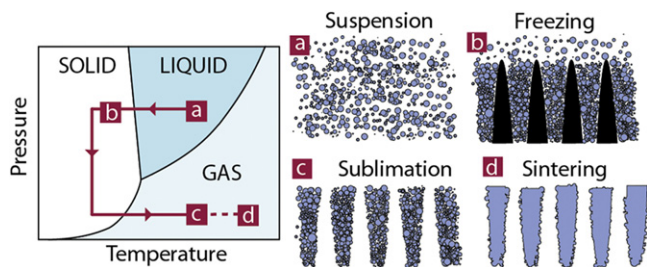


**Figure 1.** Principles of ice-templating. The colloidal suspension is frozen, the solvent crystals are then sublimated, and the resulting green body sintered.

camphene [9], tert-butyl alcohol (TBA) [10], naphthalene/camphor [11], dioxane [12], terpene [13], deep eutectic solvents [14], or carbon dioxide [15]. Various terms have been coined for the process: ice templating [16], freeze-casting [1], crystal-templating [17], directional freeze-drying [18], freeze-thaw [19] freeze gelation [20], ice-segregation-induced self-assembly [21], or thermally induced phase separation [22]. *Frozen solvent templating* [23] is probably the most generic.

Here, we performed a meta-analysis of the published structural and mechanical properties of ice-templated materials, to both provide an objective overview of the range of properties that can be achieved and to identify the critical parameters that control these properties. The combination of data and parameters from a large collection of papers [8–12, 24–142] can partially make up for the incomplete records in the literature. We use the results from this meta-analysis to derive guidelines for optimizing the structure and mechanical response of ice templated materials.

## 2. Methods

The meta-analysis was performed by manually data mining published, peer-reviewed papers or conference proceedings for various parameters describing the structural and the mechanical properties as well as the formulation of the suspensions and the characteristics of the powders. The papers analyzed cover a variety of materials including ceramics (alumina [8–11, 26, 28, 32, 36, 38, 43, 48, 54, 58, 77, 81, 89, 102, 104, 105, 111, 112, 131, 143], zirconia [49, 80, 100, 101, 103, 125–127], silicon carbide [45, 106, 130], silicon nitride [35, 69, 72, 75, 76, 79, 84, 87, 88, 128], mullite [90, 110, 124, 137], hydroxyapatite [12, 37, 44, 52, 61, 68, 78, 86, 91, 95–98, 107, 109, 113, 115, 120, 134, 135], tri-calcium phosphate [31, 40, 56, 117, 118], lead zirconate titanate (PZT) [39, 63, 74, 82, 83, 121, 122], barium titanate [73], silica/kaolinite [47], titania [24, 29, 50, 99], zirconium diboride [51], chromium carbide [42], sialon [64, 66], lithium iron phosphate [60], yttrium orthosilicate [57, 62], cermets [116, 123], cordierite [129], aluminum nitride [133], iron oxide [136], baghdadite [34]), glass and bioglass [41, 55, 85, 114, 117, 117, 132], and metals (titanium [65, 70, 92–94, 108]). The plots were digitized when the exact values were not provided directly in the text or through tables. The data were

analyzed and plotted using an IPython notebook [144]. The raw data (CSV files) as well as the IPython notebook are available from FigShare (<http://dx.doi.org/10.6084/m9.figshare.1412626>).

The pore size is not always reported. In ice templating, crystals are usually grown unidirectionally. A morphological gradient that corresponds to the initial transient regime (nucleation of the crystals and growth to reach the steady growth state) is systematically observed [145], but its dimensions are usually limited to a few hundred microns at most. It is therefore not representative of the overall microstructure, and often removed before testing. We focus here of the characteristics of the pores that correspond to the steady state growth regime. The resulting pore size is thus determined by a measurement of the cross-section of the crystals in a direction perpendicular to the main solidification direction (given by the temperature gradient).

The pore morphology strongly depends on the nature of the solvent. When water is used, the pores usually have a lamellar morphology or, more precisely, the pores are tubular with an ellipsoidal cross-section, and a strong aspect ratio between the short and long axis (figure 2). The *width* of the pore, which corresponds to the short axis of the ellipse, is usually reported. If the pores exhibit an isotropic cross-section, the pore size is given directly by the dimension of the pore in its cross-section. Since the morphology of the pores is usually maintained along the solidification direction, there is usually no need to correct the measured pore size by stereological parameters [146]. In addition, the pore size is often reported as a single number; the actual pore size distribution is seldom reported, whereas it might have a critical influence over the mechanical response.

The presence or absence of structural defects was determined by a visual inspection of the micrographs. As the most commonly encountered structural defects (described below) are usually oriented perpendicular to the main solidification direction, micrographs taken along the solidification direction are required to ascertain the presence or absence of defects. It was thus not always possible to conclude on their presence.

## 3. Results

We first look at the reported structural properties (porosity, pore size). Then, the compressive and flexural strength values are discussed, and the influence of processing and measurement parameters over these strength values is reported and analyzed.

### 3.1. Structure

For a complete description of the morphologies and typical structural features found in ice templated materials, we refer the reader to one of the reviews already published on the process [1–5, 7]. Here, we focus on the amount of porosity and the pore size, which impact the reported strength values.

The porosity is almost always measured after sintering, which reduces the pore size and content by 10–25 vol% [147]. The porosity is therefore not approaching 100% as the solid

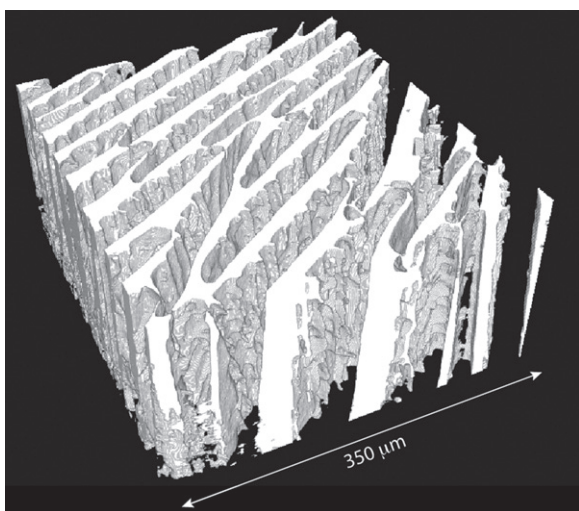


**Figure 2.** Three-dimensional reconstruction of the structure of a macroporous ice templated alumina sample (water-based suspension), obtained by x-ray computed tomography. Ice crystals were grown in the vertical direction.

loading gets close to 0 vol%. Achieving very high porosity is easier with materials that do not require sintering (polymers, graphene, nanotubes).

The total porosity is controlled, as a first-order parameter, by the initial solid loading of the suspension. Usually, the growing crystals repel all particles, additives, and impurities, and concentrate them within the inter-crystal space. The final porosity is a replica of the solvent crystals: its total content can thus be adjusted directly by the solid loading. We plotted, in figure 3, the total porosity versus the solid loading of the suspension for the three most commonly used solvents: water, camphene, and TBA.

Ice templating is a versatile and flexible process, able to yield a very wide range of porosity values, from >99.9 vol% ice-templated graphene [148, 149] for which no sintering is necessary, to almost zero [48, 133]. A transition in the morphology of the pores is observed when the solid loading is so high that the redistribution of particles by the growing crystals cannot take place anymore. The typical solid loading for this transition is around 50–55 vol% [1]. Above this critical solid loading, the low tortuosity of the individual pore channels is lost, and the pore size becomes smaller.

The range of pore size achieved is plotted in figure 4, for water, camphene, and TBA. The typical pore size range is essentially the same for all the solvents, from 4 to 500  $\mu\text{m}$ . Pores larger than 200  $\mu\text{m}$  were not found with TBA, although this limit might just be a consequence of the lower number of records.

A unique feature of ice-templating is the ability to yield directional pores with an almost constant cross-section. There is nevertheless almost always a progressive increase of the pore size as we move along the solidification direction. This increase results from the direct relationship between the growth velocity of the crystals and the pore size, and the difficulty to maintain a constant growth velocity over long distances (centimeters). A constant growth velocity can be

achieved [150] with two cold sources at each extremity of the mold and proper cooling rate profiles but has not been used very often. The main parameter that controls the pore size is the growth velocity, which results from the cooling rate and the applied temperature gradient [151]. It is therefore strongly dependent on the experimental setup used, and cannot be ascertained from this meta-analysis, as almost every paper reports a different cooling setup. The relationship between the cooling rate and interface velocity has nevertheless been already explored in detail in individual papers [45].

The relationship between the pore size and the total porosity is shown in figure 5. As expected, larger pores can be achieved for greater porosity. Figures 5 and 6, in concert, also illustrate that a trade-off between pore size, porosity, and mechanical properties can be achieved for a porosity just above 55 vol%. The achievable pore size increases rapidly when the porosity exceeds 55 vol%. Further increase of the porosity results in moderate increase of maximum pore size that can be achieved, while the strength values rapidly falls, as shown and described below (figure 6).

### 3.2. Overview of the mechanical properties: compressive and flexural strength

Two main properties of ice templated materials have been reported in the literature: the compressive strength and the flexural strength. Ice templated materials are almost always anisotropic: hence the compressive strength, along the most favorable direction, is usually reported. The flexural strength values of ice templated materials were only reported in a handful of papers.

**3.2.1. Compressive strength.** To identify the critical parameters independently of the nature of the materials used, the strength values have been normalized by the flexural strength of the corresponding dense materials. This normalization can be questioned, in particular for low porosity where the fracture mode is not primarily bending. For cellular ceramic materials under compression, the local stresses are in majority bending [152]. The structures are always imperfect, failure occurs thus always in local bending [153]. This normalization nevertheless allows a comparison of all types of materials, from very strong (zirconia, alumina, titanium), to very weak (barium titanate, calcium phosphates, etc.) materials.

We plotted the relative compressive strength versus porosity in figure 6, for all solvents. To provide a comparison with well-known morphologies, data for cellular ceramic materials [154] have been plotted on the same figure. These data have also been normalized by the flexural strength, and provide a fair overview of the mechanical properties of a wide range of ceramics materials (alumina, silicon carbide, silicon oxycarbide, titania, hydroxyapatite, and mullite) and shaping routes (polymer replica, wood replica, sacrificial templating, direct foaming with surfactants or particles). To a first approximation, there is nothing specific about the properties of directional, ice templated materials. Even if the experimental dispersion is relatively important, the compressive strength can be predicted from the porosity within an order of

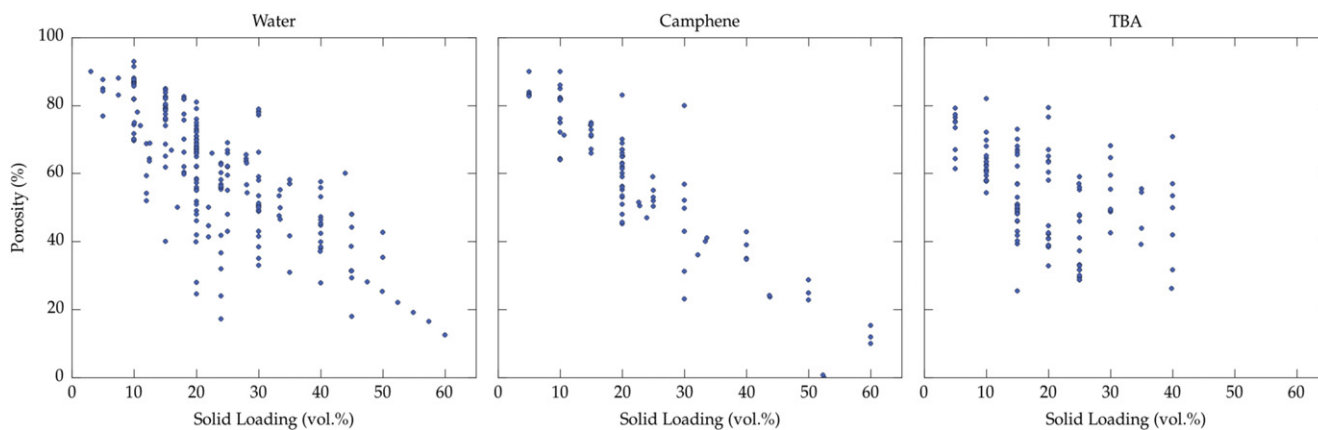


**Figure 3.** Porosity versus solid loading, for the three most commonly used solvents: water, camphene, and TBA. The porosity reported here is the total porosity of the macroporous materials after sintering.

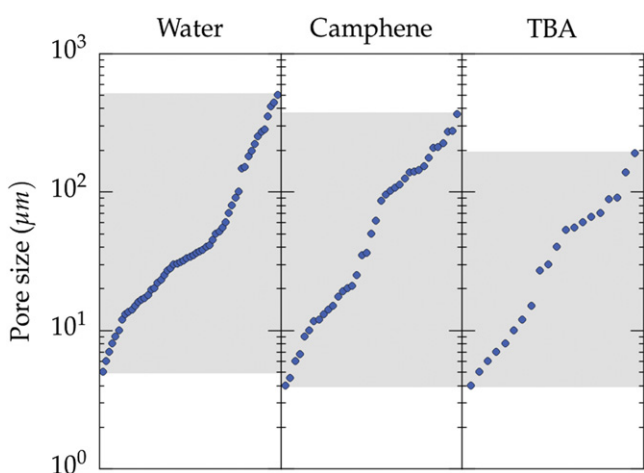


**Figure 4.** Range of pore size achieved for the three most commonly used solvents: water, camphene, and TBA. The values are simply plotted in increasing order.

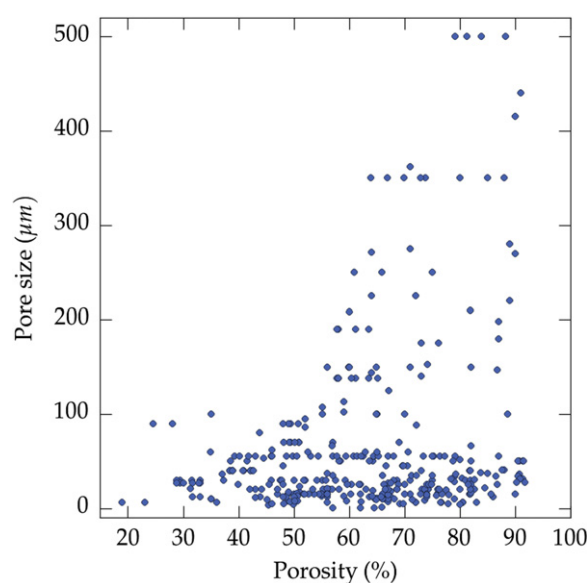


**Figure 5.** Pore size versus total porosity, all solvents reported in the papers analyzed in this meta-analysis. Large pores (>100 μm) have been rapidly obtained when the porosity exceeds 55 vol%. Small pores (<30 μm) can be obtained for all solid loadings; a fast growth velocity of the crystals is enough to achieve small dimensions.

magnitude. There are more data points at high porosity for ice templated materials, as the specific set of papers selected by Studart *et al* [154] was focused on cellular ceramics where a high porosity is usually targeted.

**3.2.2. Flexural strength.** Little flexural strength data of ice templated materials have been reported. The values, reported in figure 7, have again been normalized by the flexural strength value of the corresponding dense materials. Since less data can be found than for the compressive strength, it is thus more difficult to extract any trend from these values.

Very few data points can be found for high porosity (>70%). This absence is probably related to the difficulty of machining samples with parallel faces, and the risk of indentation by the support during the loading. The comparison of figures 6 and 7 shown that the strength values in flexion and compression are very similar, for a given porosity. The amount of porosity is therefore the first order parameter to test. There is therefore little interest to test these materials in flexion.

**3.2.3. Pore size.** The pore size seems to influence the strength of ice-templated materials (figure 8). There is again a lot of scatter of the values, resulting from variations in the formulation and process parameters, but the maximum strength that can be achieved is inversely proportional to the pore size. When the pore size is smaller than a few tens of μm (approximately 20 μm), little increase in strength is apparently found, although this is most likely just due to the paucity of data in that region. For a given pore size (e.g. 10 μm), the strength values are scattered over several orders of magnitude. It is thus clear that many other parameters have a critical influence over the mechanical properties of the ice templated materials.

**3.2.4. Failure mode.** Two failure modes can be observed for porous ceramics tested in uniaxial compression: brittle or cellular [155]. A damageable, cellular-like behavior, is

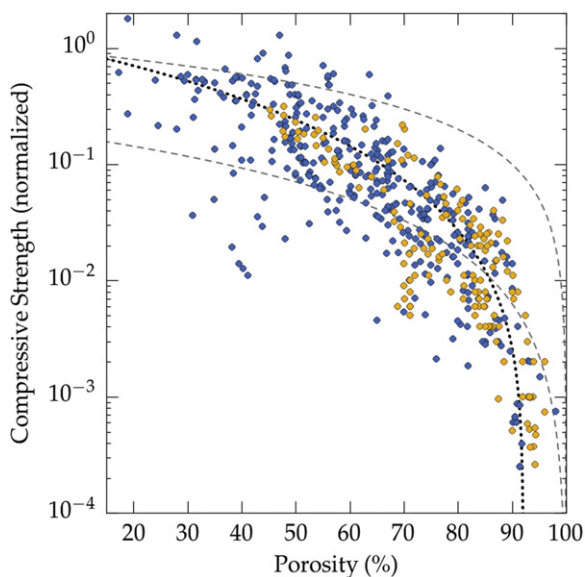


**Figure 6.** Overview of the compressive strength achieved (all materials and all solvents reported in the papers analyzed in this meta-analysis), plotted versus porosity. Color code: blue: ice templated materials, yellow: cellular ceramics from [154]. The upper and lower dashed lines correspond respectively to the closed-cell and open-cell models. The black dotted line corresponds to the best fit of a regression analysis with a power law (exponent=2.26).

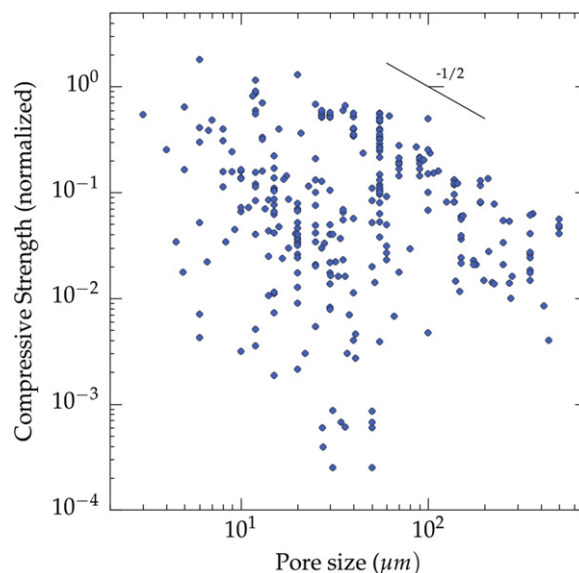


**Figure 8.** Compressive strength versus pore size (all materials and all solvents reported in the papers analyzed in this meta-analysis). Data from references [26–28, 30–47, 49, 51–54, 56–62, 64–68, 71, 73, 77–79, 85, 86, 90, 91, 94–96, 98, 100, 103–109, 118, 119, 125–127, 129, 130, 132, 134, 135].

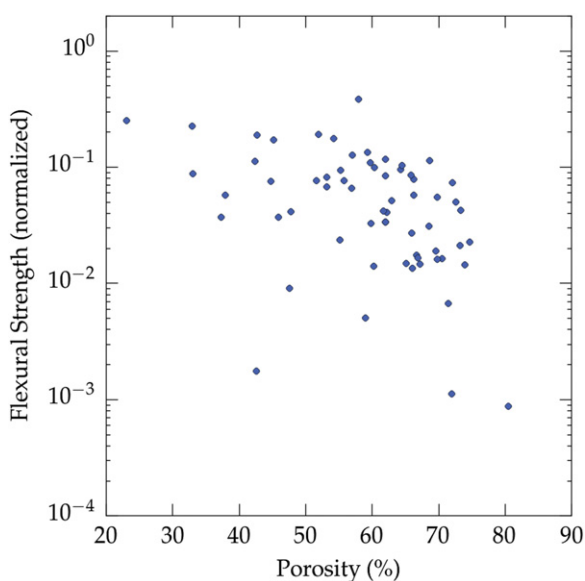


**Figure 7.** Overview of the flexural strength achieved (all materials, all solvents). Data from references [10, 26, 27, 32, 35, 47, 66, 69, 72, 75, 76, 79, 84, 87, 88, 135].

observed at high porosity (typically above 60 vol%), with a progressive densification of the material after local bending of the solid walls, while for porosity below 60 vol%, a brittle behavior is observed with long macro-crack propagation along the loading direction. With ice templated materials, the transition between the two failure modes is observed around 50 vol% (figure 9). The stress–strain curves of the mechanical tests are not reported very often, and the majority of the ice templated materials have a porosity above 50 vol%. Many

features such as the pore size, pore morphology, or density of the walls, can impact the local loading mode of the structure and its mechanical response. Therefore, we do not expect a very sharp transition between the two failure modes when such a large number of papers are analyzed. The precise determination of the transition between the failure modes would thus require additional investigations.

For isotropic porous ceramics, this transition is governed by the size of the crack initiating from the large pores and the mean distance between these pores. Here, the pore morphology is different, but the amount of stored energy favors brittle fracture at high densities. In contrast, for the lowest densities, the low amount of stored energy and the presence of defects in the microstructure favor the progressive damage of the material during compression.

**3.2.5. Structural defects.** The presence or absence of structural defects is critical to determine the overall mechanical response of the porous materials. Defects in ice templated materials are obtained under certain conditions, which, as of today, have not been clarified [156]. These defects are related to the development of so-called *ice lenses*: ice crystals growing perpendicular to the solidification direction, which adopt a crack-like morphology (figure 10). Their appearance is mostly studied in geophysics, for their occurrence is of interest to explain, in particular, the freeze-thaw cycles of frozen soils [157–159].

The most appealing hypothesis [160] invoked to explain their formation is related to the development of residual stresses during the completion of freezing (a result of the volume increase that accompanies the water to ice phase transformation), and mechanical resistance of the pack of concentrated particles between the ice crystals. The

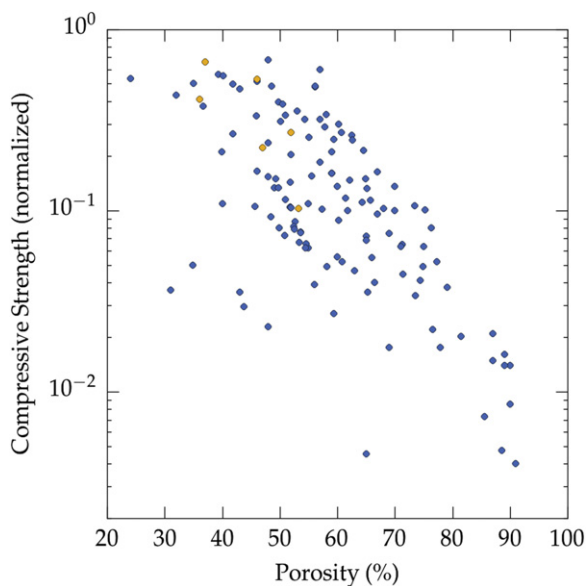


**Figure 9.** Compressive strength and failure modes (all materials and all solvents reported in the papers analyzed in this meta-analysis): brittle (yellow) [25, 64, 85] or cellular (blue) [25, 26, 28, 33, 40, 41, 51, 58, 64, 65, 70, 85, 90, 91, 94–96, 98, 103, 127, 132, 135].

morphology of the defects is indeed very similar to mechanically induced cracks [160].

It is nevertheless clear that:

- Ice-lens type defects have only been observed when water is used. This may be explained by the negligible volume change upon liquid to solid phase transformation of all the solvents used but water.
- The presence of such defects is extremely damaging for the strength of the materials, as shown in figure 11. When such defects are found, the materials is essentially pre-cracked and the resulting strength, at a given porosity, is always low compared to a defect-free (structural macro-defect) ice-templated material. Avoiding such defects is nevertheless a necessary but not sufficient condition to obtain high strength values [156], as some defect-free ice-templated materials have a low compressive strength, compared to ice-templated materials with the same porosity.

### 3.3. Suspensions properties

Several parameters are set when the initial suspension to be ice templated is prepared: nature of the solvent, solid loading, addition of processing additives such as binder or surfactants. A wide variety of processing additives have been used, it is thus not possible to extract any conclusion from this meta-analysis with regards to their possible influence. Two main parameters have been investigated here: the nature of the solvent and the particle size of the starting powder.

**3.3.1. Particle size.** The influence of the particle size over the compressive strength (for all solvents) is plotted in

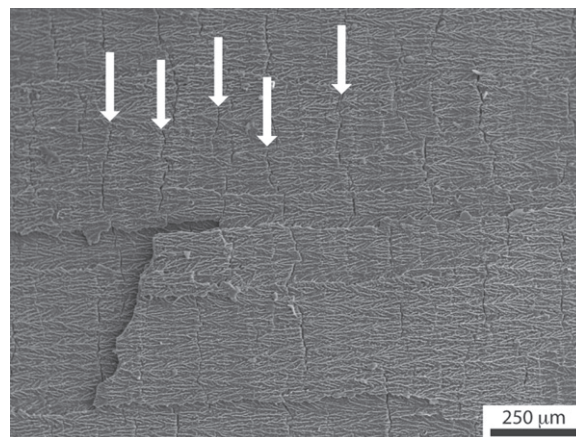


**Figure 10.** Ice-lens type defects (arrows) in ice-templated alumina. Solidification direction: left to right. Such defects appear perpendicular to the main solidification direction.

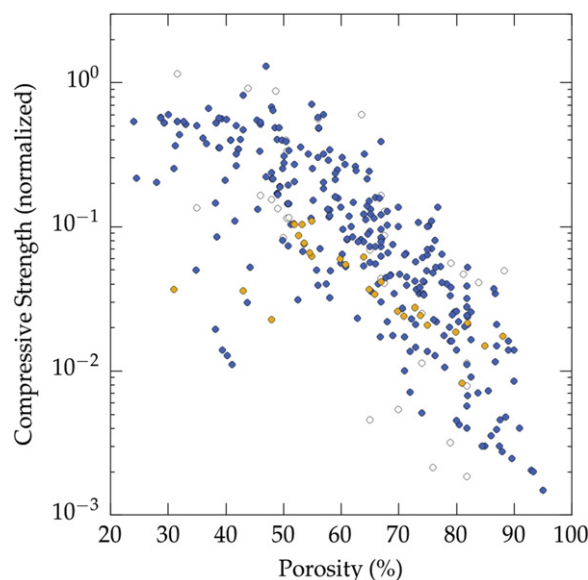


**Figure 11.** Compressive strength in presence and absence of ice-lens type structural defects (all materials and all solvents reported in the papers analyzed in this meta-analysis). Color code: blue: no defects [26–31, 33, 36, 38, 40, 41, 43, 44, 46, 50–55, 61, 64, 65, 67, 68, 70, 71, 73, 77, 78, 85, 90, 91, 94, 98, 100, 103–110, 113, 115, 118, 124–127, 129, 130, 132, 134, 135, 143], yellow: defects [25, 52, 86, 91, 96], white: cannot tell from the published micrographs [37, 39, 49, 56, 91, 95, 96, 119].

figure 12. Similar to the previous plots, a lot of scatter is observed. The most interesting information is the upper limit of what can be achieved. There seems to be an optimal range of particle size (approximately 0.5–2 μm) for which the compressive strength is maximized. This optimum may have several explanations. When large particles are used as raw materials for this processing, gravitational sedimentation of raw materials in a slurry can always occur during casting or freezing. Thus, for porous metals, ice templating has been applied mostly to titanium, because of its light density. Since the spacing between crystals is mostly given by the temperature gradient, particle size must be always smaller

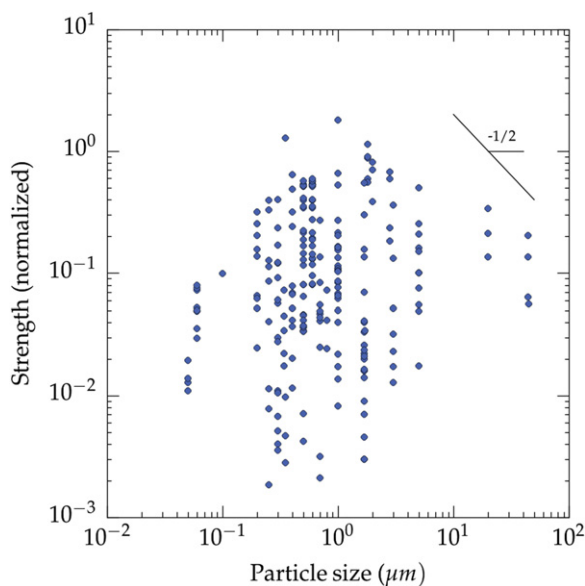


**Figure 12.** Influence of the starting particle size over the compressive strength (all materials and all solvents reported in the papers analyzed in this meta-analysis). Data from references [26–28, 31, 36–39, 46, 49, 51–53, 56, 61, 64, 65, 67, 68, 70, 71, 73, 77, 78, 85, 94–96, 103–106, 113, 118, 119, 125–127, 129, 130, 132].

than the cell wall thickness. If the particle size is larger than the average spacing between crystals, a good templating effect by the crystals cannot be achieved. Large particles are thus not very favorable.

In addition, the particle size dictates, along with the sintering conditions, the grain size in the final ceramic (or metallic) material. In ceramic and metal materials, the strength increases when the grain size decreases [161]. For ice templated materials, an increase of the particle size and hence the grain size would thus decrease the compressive strength. In addition, the grain size also plays a role on the characteristics of inter granular pores obtained after sintering. The larger the particle size, the more difficult the densification of the walls surrounding the pores. Hence, when we use larger particles (a few  $\mu\text{m}$  or more), we are more likely to end up with inter granular pores, which will act as defects when the material is put under stress/strain. The resulting strength is thus lowered.

The decrease of compressive strength when the particle size becomes lower than approximately  $0.5 \mu\text{m}$  is more difficult to explain. A possible explanation could be the role of the inter particle electrostatic forces, since ceramic particles usually exhibit a surface charge at their surface. When the particle size decreases, the magnitude of the electrostatic interactions increases. This increase may in turn affect the behavior of the particles when they are concentrated by the growing crystals, and affect the packing and thus the homogeneity of the structure by an increase of the inter-particle porosity. Again, additional experiments would be required to investigate this aspect.

**3.3.2. Role of the solvent.** The choice of the solvent is critical for the structure and properties obtained. Since the

pores are a replica of the solvent crystals, both pore morphology and pore size are dependent on the nature of the solvent. In figure 13, we plotted the normalized compressive strength for the three most commonly used solvents. The size of the markers is proportional to the pore size. Several conclusions can be drawn from these plots.

Different behaviors are observed for each solvent. With water, a lot of scatter is observed. Conversely, data with camphene and TBA show less scatter, which cannot be explained by the range of pore size that can be achieved, since it is essentially the same for all solvents (figure 4). Beyond the ice-lens defects discussed previously, the scatter with water can be partly explained by the wider range of pore morphology that can be achieved with water-based suspensions. Ice growth is very sensitive to the nature and characteristics of common ceramic processing additives (dispersant, binder, etc) [163]. Morphologies typical of that obtained with several solvents are shown in figure 14. The growth behavior of camphene and TBA crystals is apparently a lot more robust. The crystals morphology is less sensitive to the formulation and process parameters. The pore size data also provide useful observations. For high porosity (above 60 vol%), large pores yield higher compressive strength values, but only when water is used. This increase possibly results from the greater thickness of the walls between the pores, which are therefore less sensitive to structural defects. For lower porosity (below 60 vol%), smaller pores result in higher compressive strength values. For camphene and TBA, this is not evident, possibly because of the relative paucity of data for these solvents.

### 3.4. Measurement conditions

The conditions under which the mechanical properties are measured are also critical, and determine, to a large extent, the absolute values obtained. Even though standard test methods and good practices exist, they are not systematically followed. The strain rate, the sample volume, the sample aspect ratio, the experimental setups, the surface preparation: all of these parameters affect, to some extent, the measured compressive strength. More subtle parameters, such as the presence of a pad (typically cardboard) between the sample and the testing setup to ensure a good alignment of the sample along the loading direction, are very rarely reported although they may also affect the results. We analyzed the influence of the strain rate, sample volume, and sample aspect ratio. There is too much scatter (due, in part, to all the parameters described in the previous sections) in the values reported here, so no clear trend could be observed with the current meta-analysis. Some of these parameters have been investigated in previous papers (see for instance the effect of loading rate reported in figure 6 of Fu *et al* [96]).

## 4. Discussion

### 4.1. Prediction by the mechanical models

Several models have been developed, in particular by Ashby, Medalist, and Gibson [153, 164], to predict the mechanical



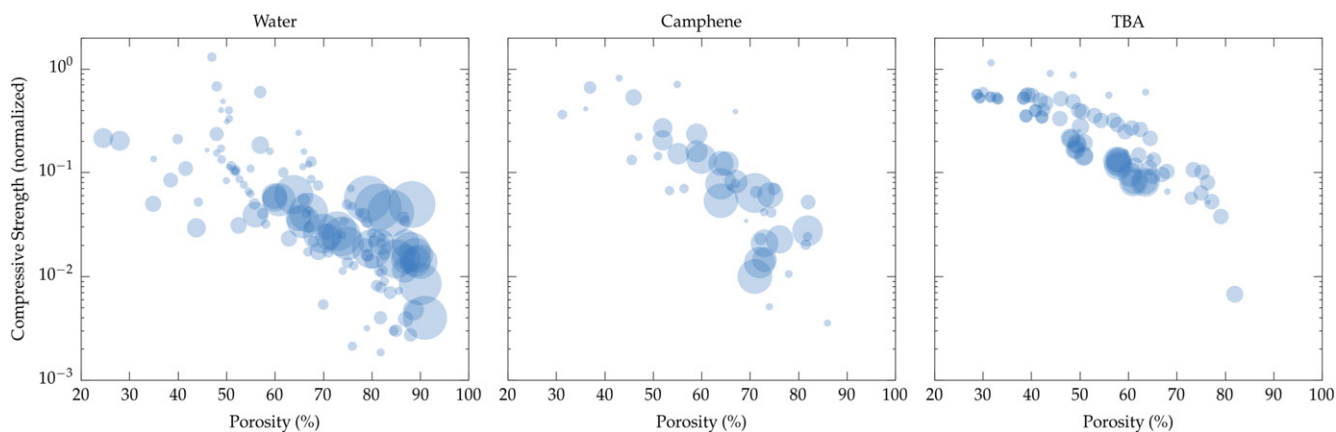


**Figure 13.** Influence of the nature of the solvent over the compressive strength. References for the data: water [8, 12, 26, 27, 31, 33–38, 43–49, 51, 52, 55–61, 68, 69, 72–76, 81, 84, 86–92, 94–101, 103, 104, 111, 113, 116, 119, 124, 128–132, 134, 135], camphene [9, 29, 30, 42, 50, 64–67, 70, 80, 85, 93, 102, 105–109, 114, 115, 117, 118, 120–123, 125–127, 136], TBA [10, 32, 39–41, 53, 62, 63, 71, 77, 78, 82, 83, 110, 137]. The marker size is proportional to the pore size.

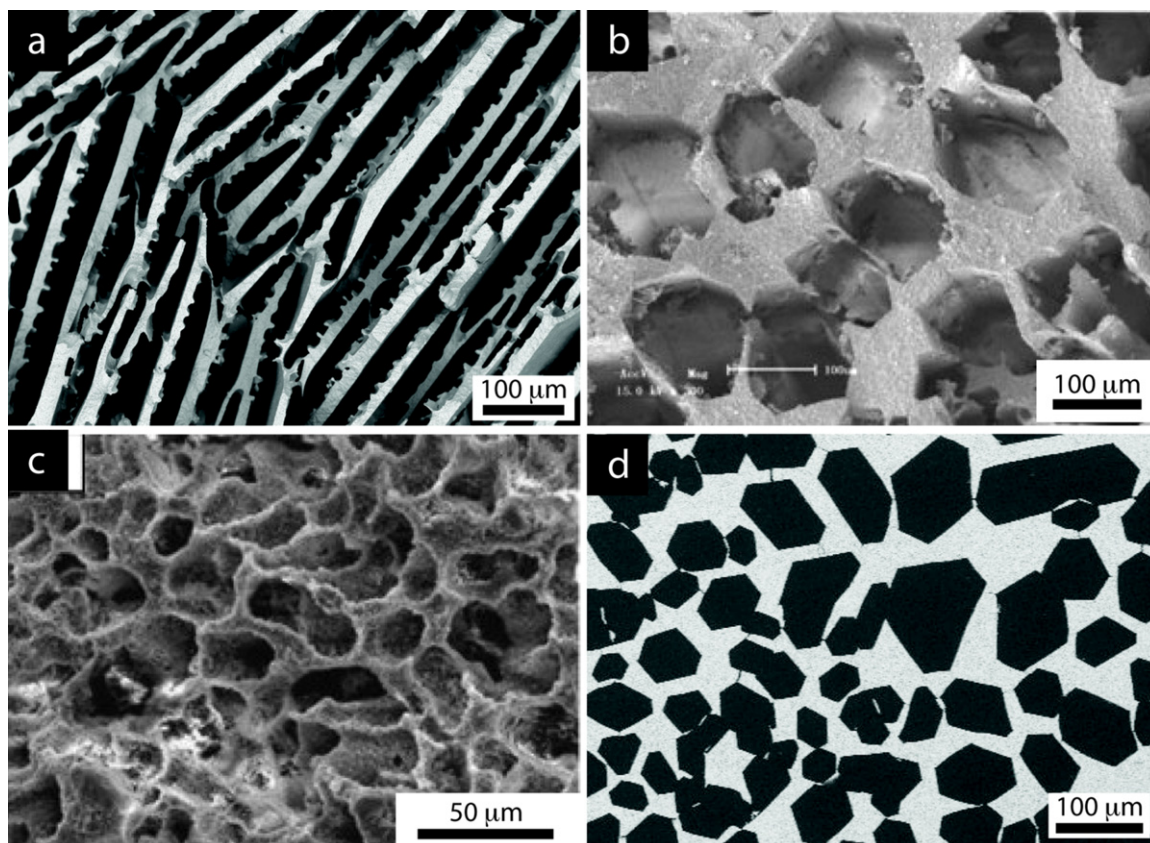


**Figure 14.** Porous structures representative of what can be achieved with (a) water, (b) TBA, (c) camphene, and (d) water with additives (zirconium acetate). Credits: (b) reprinted from [162], Copyright (2010), with permission from Elsevier, (c) reprinted from [125], Copyright (2010), with permission from Elsevier.

response of cellular solids with various morphologies (figure 15). The open- and closed-cell foam models, in particular, are very often used to understand and predict the behavior of cellular materials. These models predict the following values for the compressive strength.

- Closed-cell

$$\sigma = \sigma_p \left( C_6 \left( \phi \frac{\rho^*}{\rho_s} \right) + C_6'' (1 - \phi) \frac{\rho^*}{\rho_s} \right), \quad (1)$$

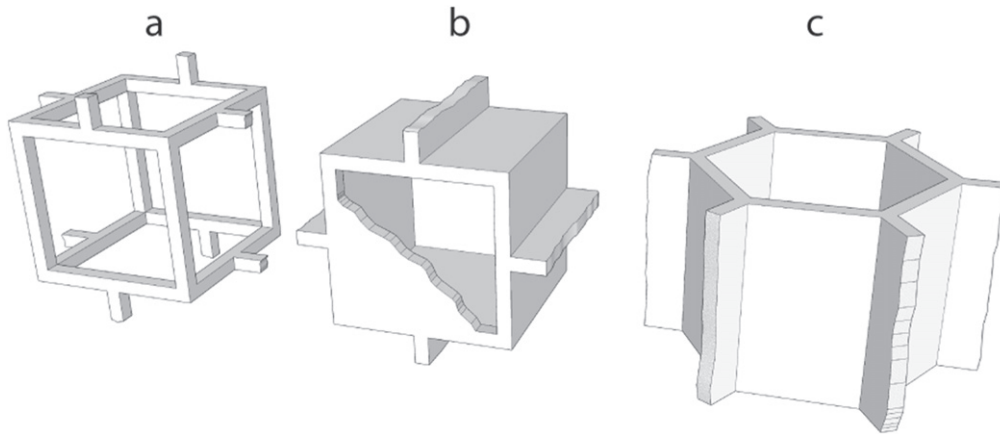


**Figure 15.** Morphology of the foam cells of the Ashby, Medalist, and Gibson [153, 164] models: (a) open-cell, (b) closed-cell, (c) honeycomb.

with  $C_6 = 0.65$  and  $C_6' = 1$ , and where  $\phi$  is the solid fraction in the edges,  $\rho_s$  and  $\rho^*$  the apparent density of the dense and cellular material respectively, and  $\sigma_p$  the modulus of rupture of the solid cell wall material.

- Open-cell (brittle crushing mode)

$$\sigma = \sigma_p C_4 \left( \frac{\rho^*}{\rho_s} \right)^{3/2}, \quad (2)$$

with  $C_4 = 0.2$ , and where  $\sigma_p$  is the modulus of rupture of the solid cell wall material, and  $\rho_s$  and  $\rho^*$  the apparent density of the dense and cellular material respectively.

- Honeycomb, out of plane

$$\sigma = 6E_s \left( \frac{\rho^*}{\rho_s} \right)^3, \quad (3)$$

where  $E_s$  is Young’s modulus of the corresponding dense material, and  $\rho_s$  and  $\rho^*$  the apparent density of the dense and cellular material respectively.

As shown on figure 6, the first two models do not provide a good description of the behavior of ice template materials. The variation of the compressive strength with porosity does not follow the prediction of models for open- and closed-cell foams. Those models are well fitted for the prediction of mechanical properties of ceramic foams, because the cell walls in the foams are not continuous (they are divided by pores, similar to that of open cell model).

The morphology of ice templated materials—continuous pores, with an almost constant cross-section—is actually a lot closer to that of a honeycomb (figure 14). We plotted in figure 16 the measured compressive strength versus the compressive strength predicted by the honeycomb out-of-plane model [165] for water, camphene, and TBA. Although these three solvents yield crystals with very different morphologies, the high pore directionality makes the honeycomb model a good descriptor of the structure and indeed the observed strength.

The camphene crystals (figure 14(c)) have a dendritic morphology [166]. That makes them less similar to the ideal honeycomb structure. This effect causes a disparity between the predicted and experimental values (figure 14(b)), particularly at high porosities where the growth of secondary arms (dendrites) is more important.

TBA crystals (figure 14(b)), on the other hand, are hexagonal and usually continuous along the solidification direction [53, 78, 162]. The agreement between the measured and predicted properties in this case is surprisingly good. This behavior may probably be extended to water crystals, when they adopt hexagonal morphologies (figure 14(d)) in the presence of zirconium acetate [167].

The case of water deserves special attention. Even though the lamellar morphology with some degree of surface roughness does not resemble the honeycomb, the predictions from honeycomb are in reasonable agreement with the experimental values (figure 14(a)), mainly because the predominant solicitation in both cases is Euler buckling [168]. Nevertheless, there is still a lot of scatter in the data. This scatter may come from two different sources. First, although the same failure mechanism was observed, the stress distribution in the struts might be different for both morphologies. Then, as mentioned previously, ice crystals are more sensitive to the addition of additives, which may affect the directionality of pores and the generation of structural defects.

In addition, in the use of the honeycomb model, the density of the ‘dense’ material is not corrected for wall porosity, as might be the case for large particle sizes. This is difficult to estimate without a measurement of the porosity in the wall, which is almost never mentioned or reported. This might account for some of the scatter in the prediction.

#### 4.2. Missing data and the difficulty of systematic comparison

The current meta analysis underlines again the crucial importance of reporting all the process and experimental parameters, and, whenever possible, a complete structural and

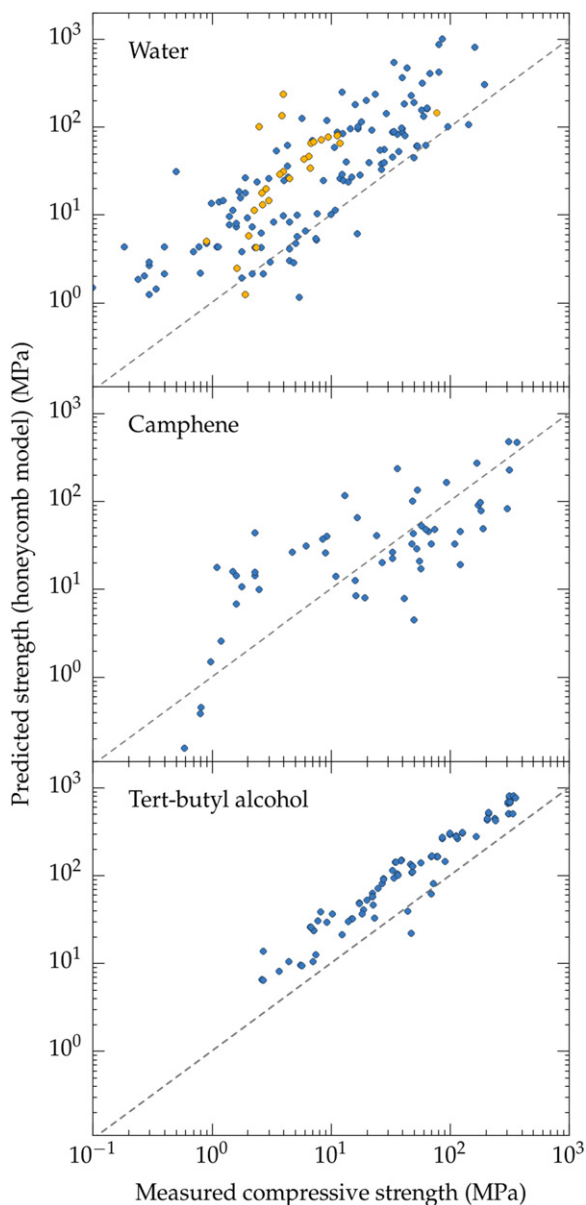


**Figure 16.** Compressive strength: measured (all materials reported in the papers analyzed in this meta-analysis) versus predicted by Ashby honeycomb out-of-plane model. The dashed line corresponds to the predictions of the model. Color code: blue, no defects; yellow: ice-lens type defects.

mechanical characterization. We believe a meta-analysis provides an objective view of what we may achieve in terms of structure and properties. Nevertheless, such analysis, and any other systematic comparison, is more easily performed and more reliable if all parameters and properties are carefully documented in every paper. Unfortunately, each author has its own habits for reporting results. The solid loading of the suspension, for instance, can be reported either in weight or volume percent, and computed with or without the other processing additives (binder, dispersant). The materials are often not fully characterized, and key information is often missing. Systematic comparisons are therefore more difficult.

#### 4.3. Which conditions are the best ones?

This, of course, depends on what one wants to achieve in terms of structural or functional properties. The following lessons can be learned from the current meta analysis.

- The targeted range of pore size should not dictate the choice of the solvent, as all of the most popular solvents (water, camphene, TBA) can fulfill a very similar range of pore size (4–500  $\mu\text{m}$ ). The morphology of the pores can nevertheless be a criterion that dictates the choice of the solvent, in particular if certain functional properties are targeted. The dendritic surface features aligned along the growth direction of ice crystals, for instance, can be beneficial [169] for neurite growth.
  - There is apparently an optimal range of particle size (approximately 0.5–2  $\mu\text{m}$ ) for which the compressive strength is maximal. The reason for this optimum is not clear.
  - It is less robust to work with water-based suspensions than with camphene or TBA. The growth of ice crystals is more sensitive to impurities, formulation, and process parameters. Using water therefore requires a good understanding of the process and the various parameters involved.
  - The open- and closed-cell foam mechanical models are not appropriate to predict the behavior of these cellular materials. The honeycomb model of Zhang and Ashby [165], however, accurately predicts the behaviors of TBA crystals-templated samples.
  - The influence of the pore size on the mechanical response is complex. For high porosity of water-based samples, larger pores are more likely to yield a high compressive strength. For low porosity (all solvents), smaller pores are preferable.
  - A trade-off between large pore size and mechanical properties can be achieved for a porosity above 55 vol%. Such trade-off is often critical in applications like tissue engineering, where large pores are required and yet the materials must be able to sustain a certain level of load. The achievable pore size increases rapidly when the porosity exceeds 55 vol%. Further increase of the porosity results in a moderate increase of the pore size, while the strength rapidly decreases (figure 6). To achieve both large pores (>200  $\mu\text{m}$ ) and high strength (50% of the strength of the corresponding dense material), the optimal porosity is therefore in the 60–65 vol% range. It is very likely that this trade-off can be further optimized towards higher strength by a careful process and structural control.
- A lot of work remains to be done to fully understand the behavior and the range of properties that can be achieved with ice-templated materials. The following points probably deserve more attention in future work.
- The Weibull modulus (which requires a very large number of samples), has just been reported in one study

[170], and yet is critical to predict the reliability of these materials, in particular for structural applications.

- The detailed identification of the transition between the brittle and cellular failure modes could be determined more precisely. This understanding will be helpful to select the proper mechanical response based on the functional requirements of the targeted application.
- These materials are almost always anisotropic. The direction that provides the best mechanical response is almost always tested; a lot could be learned from testing the materials in their weak direction. Fu *et al* [96], for instance, reported a strength ratio of three between strong and weak directions.
- The role of the pore size distribution over the mechanical response has not been investigated and might play a critical role for the mechanical response and failure behavior. To have a better understanding of the influence of the solid phase (respectively the porosity) morphology, on the mechanical properties, a quantitative study has to be carried out. The use of 3D volumes from x-ray computed tomography, coupled with a finite elements simulation [171] or with discrete element modeling [172] are powerful approaches.

## 5. Conclusions and recommendations

Ice templating is a rich processing route, with many formulation and process parameters, which can be used with practically any material. This versatility nevertheless results in added complexity. It is essential to have a good understanding of the process and the influence of the formulation, freezing, and testing parameters. We hope that this meta-analysis will be a helpful guide to anyone interested in working with such materials in order to optimize their relative mechanical strength.

We also insist that it is essential to report properly all the experimental parameters and results, and in a way that can be easily reused by anyone else. It is, for instance, much easier to extract values from tables than from plots. Until data repositories become standard and data mining can be automated, it is therefore a good practice to include both tables and plots.

## Acknowledgments

The research leading to these results has received funding from the European Research Council under the European Union's Seventh Framework Programme (FP7/2007-2013)/ERC grant agreement 278004 (project FreeCo). JS has been supported by the CNRS and Saint-Gobain under BDI grant agreement 084877 for the Institut National de Chimie (INC).

## References

- [1] Deville S 2008 Freeze-casting of porous ceramics: a review of current achievements and issues *Adv. Eng. Mater.* **10** 155–69
- [2] Deville S 2010 Freeze-casting of porous biomaterials: structure, properties and opportunities *Materials (Basel)* **3** 1913–27
- [3] Wegst U G K, Schecter M, Donius A E and Hunger P M 2010 Biomaterials by freeze casting *Phil. Trans. R. Soc. A* **368** 2099–121
- [4] Li W L, Lu K and Walz J Y 2012 Freeze casting of porous materials: review of critical factors in microstructure evolution *Int. Mater. Rev.* **57** 37–60
- [5] Deville S 2013 Ice-templating, freeze casting: beyond materials processing *J. Mater. Res.* **28** 2202–19
- [6] Fukushima M, Yoshizawa Y-I and Ohji T 2014 Macroporous ceramics by gelation-freezing route using gelatin *Adv. Eng. Mater.* **16** 607–20
- [7] Pawelec K M, Husmann A, Best S M and Cameron R E 2014 Ice-templated structures for biomedical tissue repair: from physics to final scaffolds *Appl. Phys. Rev.* **1** 021301
- [8] Fukasawa T, Deng Z and Ando M 2001 Pore structure of porous ceramics synthesized from water-based slurry by freeze-dry process *J. Mater. Sci.* **6** 2523–7
- [9] Araki K and Halloran J W 2004 New freeze-casting technique for ceramics with sublimable vehicles *J. Am. Ceram. Soc.* **87** 1859–63
- [10] Chen R, Wang C-A, Huang Y, Ma L and Lin W 2007 Ceramics with special porous structures fabricated by freeze-gelcasting: using tert-butyl alcohol as a template *J. Am. Ceram. Soc.* **90** 3478–84
- [11] Araki K and Halloran J W 2004 Room-temperature freeze casting for ceramics with nonaqueous sublimable vehicles in the naphthalene–camphor eutectic system *J. Am. Ceram. Soc.* **2019** 2014–9
- [12] Rahaman M N and Fu Q 2008 Manipulation of porous bioceramic microstructures by freezing of suspensions containing binary mixtures of solvents *J. Am. Ceram. Soc.* **91** 4137–40
- [13] Tomeckova V and Halloran J W 2012 Porous ceramics by photopolymerization with terpene-acrylate vehicles ed L Gauckler *J. Am. Ceram. Soc.* **95** 3763–8
- [14] Gutiérrez M C, Ferrer M L, Yuste L, Rojo F and Monte F D 2010 Bacteria incorporation in deep-eutectic solvents through freeze-drying *Angew. Chem., Int. Ed. Engl.* **49** 2158–62
- [15] Zhang H, Long J and Cooper A I 2005 Aligned porous materials by directional freezing of solutions in liquid CO<sub>2</sub> *J. Am. Chem. Soc.* **127** 13482–3
- [16] Gutiérrez M C, Jobbagy M, Ferrer M L and Monte F D 2008 Enzymatic synthesis of amorphous calcium phosphate–chitosan nanocomposites and their processing into hierarchical structures *Chem. Mater.* **20** 11–3
- [17] Guizard C, Leloup J and Deville S 2014 Crystal templating with mutually miscible solvents: a simple path to hierarchical porosity *J. Am. Ceram. Soc.* **97** 2020–3
- [18] He H *et al* 2012 Aligned porous conductive carbon black/polyvinyl alcohol composite obtained by directional freeze-drying *J. Funct. Mater.* **43** 130
- [19] Nakagawa K, Maebashi S and Maeda K 2010 Freeze-thawing as a path to concentrate aqueous solution *Sep. Purif. Technol.* **73** 403–8
- [20] Mukai S R 2003 Porous properties of silica gels with controlled morphology synthesized by unidirectional freeze-gelation *Microporous Mesoporous Mater.* **63** 43–51
- [21] Zhang X, Li C and Luo Y 2011 Aligned/unaligned conducting polymer cryogels with three-dimensional

- macroporous architectures from ice-segregation-induced self-assembly of PEDOT-PSS *Langmuir* **27** 1915–23
- [22] Olivás-Armendáriz I, García-Casillas P E, Martínez-Sánchez R, Martínez-Villafañe A and Martínez-Pérez C 2010 Chitosan/MWCNT composites prepared by thermal induced phase separation *J. Alloys Compd* **495** 592–5
- [23] Ahmed A, Hasell T, Clowes R, Myers P, Cooper A I and Zhang H 2015 Aligned macroporous monoliths with intrinsic microporosity via a frozen-solvent-templating approach *Chem. Commun. (Camb.)* **51** 1717–20
- [24] Li W, Porter M M, Olefsky E A, German R M and Mckittrick J 2015 Sintering of bi-porous titanium dioxide scaffolds: experimentation, modeling and simulation *Mater. Sci. Eng. A* **636** 148–56
- [25] Ping R-F G, Chang S and Fu S Y-J 2015 Effects of composition and sintering temperature on the structure and compressive property of the lamellar Al<sub>2</sub>O<sub>3</sub>-ZrO<sub>2</sub> scaffolds prepared by freeze casting *J. Mater. Sci.* **50** 5039–46
- [26] Shen P, Xi J, Fu Y, Shaga A, Sun C and Jiang Q 2014 Preparation of high-strength Al-Mg-Si/Al<sub>2</sub>O<sub>3</sub> composites with lamellar structures using freeze casting and pressureless infiltration techniques *Acta Metall. Sin. Engl. Lett.* **27** 944–50
- [27] Yang H, Ye F, Liu Q, Liu S, Gao Y and Liu L 2015 A novel silica aerogel/porous Si<sub>3</sub>N<sub>4</sub> composite prepared by freeze casting and sol-gel impregnation with high-performance thermal insulation and wave-transparent *Mater. Lett.* **138** 135–8
- [28] Vijayan S, Narasimman R and Prabhakaran K 2015 Freeze gelcasting of naphthalene-in-aqueous alumina slurry emulsions for the preparation of macroporous alumina ceramics *Ceram. Int.* **41** 1487–94
- [29] Xing Z, Zhou W, Du F, Zhang L, Li Z, Zhang H and Li W 2014 Facile synthesis of hierarchical porous TiO<sub>2</sub> ceramics with enhanced photocatalytic performance for micropolluted pesticide degradation *ACS Appl. Mater. Interfaces* **6** 16653–60
- [30] Lee J, Yang T, Yoon S, Kim B and Park H 2010 Recycling of coal fly ash for fabrication of porous mullite composite *Adv. Mater. Res.* **156-7** 1649–52
- [31] Flauder S, Gbureck U and Müller F A 2014 Structure and mechanical properties of  $\beta$ -TCP scaffolds prepared by ice-templating with preset ice front velocities *Acta Biomater.* **10** 5148–55
- [32] Souza D F, Nunes E H, Pimenta D S, Vasconcelos D C, Nascimento J F, Grava W, Houmard M and Vasconcelos W L 2014 Synthesis and structural evaluation of freeze-cast porous alumina *Mater. Charact.* **96** 183–95
- [33] Kumar A, Negi Y S, Choudhary V and Bhardwaj N K 2014 Microstructural and mechanical properties of porous biocomposite scaffolds based on polyvinyl alcohol, nano-hydroxyapatite and cellulose nanocrystals *Cellulose* **21** 3409–26
- [34] Sadeghpour S, Amirjani A, Hafezi M and Zamanian A 2014 Fabrication of a novel nanostructured calcium zirconium silicate scaffolds prepared by a freeze-casting method for bone tissue engineering *Ceram. Int.* **40** 16107–14
- [35] Hu H-L, Zeng Y-P, Xia Y-F, Yao D-X and Zuo K-H 2014 High-strength porous Si<sub>3</sub>N<sub>4</sub> ceramics prepared by freeze casting and silicon powder nitridation process *Mater. Lett.* **133** 285–8
- [36] Tang Y, Miao Q, Qiu S, Zhao K and Hu L 2014 Novel freeze-casting fabrication of aligned lamellar porous alumina with a centrosymmetric structure *J. Eur. Ceram. Soc.* **34** 4077–82
- [37] Cheng Z, Zhao K, Zhang W and Guo C 2014 Preparation of hydroxyapatite scaffolds via freeze-casting using hydrogen peroxide/distilled water *J. Chin. Ceram. Soc.* **42** 672–6
- [38] Zeng J, Zhang Y, Zhou K-C and Zhang D 2014 Effects of alcohol additives on pore structure and morphology of freeze-cast ceramics *Trans. Nonferr. Met. Soc. China* **24** 718–22
- [39] Xu T and Wang C-A 2014 Piezoelectric properties of a pioneering 3-1 type PZT/epoxy composites based on freeze-casting processing *J. Am. Ceram. Soc.* **97** 1511–6
- [40] Kim D-H, Kim K-L, Chun H-H, Kim T-W, Park H-C and Yoon S-Y 2014 *In vitro* biodegradable and mechanical performance of biphasic calcium phosphate porous scaffolds with unidirectional macro-pore structure *Ceram. Int.* **40** 8293–300
- [41] Kim T W, Ryu S C, Kim B K, Yoon S Y and Park H C 2014 Porous hydroxyapatite scaffolds containing calcium phosphate glass-ceramics processed using a freeze/gel-casting technique *Met. Mater. Int.* **20** 135–40
- [42] Dong Z, Zhang Q and Chen W 2014 Fabrication of highly porous chromium carbide with multiple pore structure *J. Am. Ceram. Soc.* **97** 1317–25
- [43] Ai T, Wang F, Feng X and Zhang Y Porous Al<sub>2</sub>O<sub>3</sub> ceramics fabricated by freeze-casting using ice template *Preprint*
- [44] Farhangdoust S, Rabiee S M, Zamanian A, Yasaei M, Khorami M and Hafezi-Ardakani M 2012 Evaluating initial content of the slurry and cooling rate on the microstructural and mechanical characteristics of freeze casted hydroxyapatite macroporous scaffolds *Key Eng. Mater.* **529-530** 147–52
- [45] Naglieri V, Bale H a, Gludovatz B, Tomsia A P and Ritchie R O 2013 On the development of ice-templated silicon carbide scaffolds for nature-inspired structural materials *Acta Mater.* **61** 6948–57
- [46] Ghazanfari S M H and Zamanian A 2013 Phase transformation, microstructural and mechanical properties of hydroxyapatite/alumina nanocomposite scaffolds produced by freeze casting *Ceram. Int.* **39** 9835–44
- [47] Li W, Lu K and Walz J Y 2013 Effects of solids loading on sintering and properties of freeze-cast kaolinite-silica porous composites *J. Am. Ceram. Soc.* **96** 1763–71
- [48] Sofie S W and Dogan F 2004 Freeze casting of aqueous alumina slurries with glycerol *J. Am. Ceram. Soc.* **84** 1459–64
- [49] Liu G and Button T W 2013 The effect of particle size in freeze casting of porous alumina-zirconia composite *Ceram. Int.* **39** 8507–12
- [50] Xing Z, Li J, Wang Q, Zhou W, Tian G, Pan K, Tian C, Zou J and Fu H 2013 A floating porous crystalline TiO<sub>2</sub> ceramic with enhanced photocatalytic performance for wastewater decontamination *Eur. J. Inorg. Chem.* **2013** 2411–7
- [51] Landi E, Sciti D, Melandri C and Medri V 2013 Ice templating of ZrB<sub>2</sub> porous architectures *J. Eur. Ceram. Soc.* **33** 1599–607
- [52] Zhang Y, Zhou K, Bao Y and Zhang D 2013 Effects of rheological properties on ice-templated porous hydroxyapatite ceramics *Mater. Sci. Eng. C* **33** 340–6
- [53] Choi H-J, Lee J-H, Yoon S-Y, Kim B K and Park H-C 2012 The microstructure and properties of porous alumina/zirconia composites fabricated by a TBA-based freeze casting route *J. Ceram.* **13** 762–6
- [54] Hunger P M, Donius A E and Wegst U G K 2013 Structure-property-processing correlations in freeze-cast composite scaffolds *Acta Biomater.* **9** 6338–48
- [55] Ishikawa K, Iwamoto Y, Zamanian A, Farhangdoust S, Yasaei M, Khorami M and Abbasabadi M 2012 The effect of sintering temperature on the microstructural and mechanical characteristics of hydroxyapatite macroporous scaffolds prepared via freeze-casting *Key Eng. Mater.* **529-530** 133–7

- [56] Flauder S, Gbureck U, Müller F a, Ishikawa K and Iwamoto Y 2012  $\beta$ -TCP scaffolds with an interconnected and aligned porosity fabricated via ice-templating *Key Eng. Mater.* **529–530** 129–32
- [57] Zhang R, Fang D, Chen X, Pei Y, Wang Z and Wang Y 2013 Microstructure and properties of highly porous  $Y_2SiO_5$  ceramics produced by a new water-based freeze casting *Mater. Des.* **46** 746–50
- [58] Hunger P M, Donius A E and Wegst U G K 2013 Platelets self-assemble into porous nacre during freeze casting *J. Mech. Behav. Biomed. Mater.* **19** 87–93
- [59] Li W, Lu K and Walz J Y 2012 Fabrication of porous nanocomposites with controllable specific surface area and strength via suspension infiltration *Langmuir* **28** 16423–9
- [60] Hamamoto K, Fukushima M, Mamiya M, Yoshizawa Y, Akimoto J, Suzuki T and Fujishiro Y 2012 Morphology control and electrochemical properties of  $LiFePO_4/C$  composite cathode for lithium ion batteries *Solid State Ion.* **225** 560–3
- [61] Farhangdoust S, Zamanian A, Yasaei M and Khorami M 2013 The effect of processing parameters and solid concentration on the mechanical and microstructural properties of freeze-casted macroporous hydroxyapatite scaffolds *Mater. Sci. Eng. C* **33** 453–60
- [62] Hou Z, Liu J, Du H, Xu H, Guo A and Wang M 2012 Preparation of porous  $Y_2SiO_5$  ceramics with relatively high compressive strength and ultra-low thermal conductivity by a TBA-based gel-casting method *Ceram. Int.* **28** 799–802
- [63] Xu T T T, Wang C A C and Guo R 2012 Microstructure and electrical properties of porous PZT ceramics with unidirectional pore channel structure fabricated by freeze-casting *Key Eng. Mater.* **512–515** 1347–50
- [64] Hou Z, Ye F, Liu L and Liu Q 2012 Fabrication of gradient porous  $\beta$ -SiAlON ceramics via a camphene-based freeze casting process *Mater. Sci. Eng. A* **558** 742–6
- [65] Jung H-D, Yook S-W, Jang T-S, Li Y, Kim H-E and Koh Y-H 2013 Dynamic freeze casting for the production of porous titanium (Ti) scaffolds *Mater. Sci. Eng. C* **33** 59–63
- [66] Hou Z, Ye F, Liu L, Liu Q and Zhang H 2013 Effects of solid content on the phase assemblages, mechanical and dielectric properties of porous  $\alpha$ -SiAlON ceramics fabricated by freeze casting *Ceram. Int.* **39** 1075–9
- [67] Du J, Zhang X, Hong C and Han W 2013 Microstructure and mechanical properties of  $ZrB_2$ -SiC porous ceramic by camphene-based freeze casting *Ceram. Int.* **39** 953–7
- [68] Zhang Y, Zhou K, Zhang X and Zhang D 2011 Porous hydroxyapatite ceramics fabricated by an ice templating process *Chin. J. Mater. Res.* **25** 289–94
- [69] Zhang R, Fang D, Chen X and Pei Y 2012 Effect of pre-oxidation on the microstructure, mechanical and dielectric properties of highly porous silicon nitride ceramics *Ceram. Int.* **38** 6021–6
- [70] Yook S-W, Jung H-D, Park C-H, Shin K-H, Koh Y-H, Estrin Y and Kim H-E 2012 Reverse freeze casting: a new method for fabricating highly porous titanium scaffolds with aligned large pores *Acta Biomater.* **8** 2401–10
- [71] Choi H J, Yang T-Y, Yoon S Y, Kim B K and Park H C 2012 Porous alumina/zirconia layered composites with unidirectional pore channels processed using a tertiary-butyl alcohol-based freeze casting *Mater. Chem. Phys.* **133** 16–20
- [72] Zhang R, Fang D, Pei Y and Zhou L 2012 Microstructure, mechanical and dielectric properties of highly porous silicon nitride ceramics produced by a new water-based freeze casting *Ceram. Int.* **38** 1–5
- [73] Liu G, Button T W and Zhang D 2014 Lamellar  $BaTiO_3$  and its composites fabricated by the freeze casting technique *J. Eur. Ceram. Soc.* **34** 4083–8
- [74] Guo R, Wang C-A, Yang A and Fu J 2010 Enhanced piezoelectric property of porous lead zirconate titanate ceramics with one dimensional ordered pore structure *J. Appl. Phys.* **108** 124112
- [75] Yao D, Xia Y, Zeng Y-P, Zuo K-H and Jiang D 2012 Fabrication porous  $Si_3N_4$  ceramics via starch consolidation–freeze drying process *Mater. Lett.* **68** 75–7
- [76] Xia Y, Zeng Y-P and Jiang D 2012 Microstructure and mechanical properties of porous  $Si_3N_4$  ceramics prepared by freeze-casting *Mater. Des.* **33** 98–103
- [77] Li D and Li M 2011 Preparation of porous alumina ceramic with ultra-high porosity and long straight pores by freeze casting *J. Porous Mater.* **19** 345–9
- [78] Kim J H, Lee J H, Yang T Y, Yoon S Y, Kim B and Park H C 2011 TBA-based freeze/gel casting of porous hydroxyapatite scaffolds *Ceram. Int.* **37** 2317–22
- [79] Yue J, Dong B and Wang H 2011 Porous  $Si_3N_4$  fabricated by phase separation method using benzoic acid as pore-forming agent ed P Colombo *J. Am. Ceram. Soc.* **94** 1989–91
- [80] Han J, Hong C, Zhang X, Du J and Zhang W 2009 Microstructure controlling and properties of highly porosity ceramics by freeze-casting *ICCE-17: Proc. 17th Int. Conf. Composites or Nanoengineering* (Honolulu, HI: The Institute of Materials, Minerals, Mining)
- [81] Mongkolkachit C, Wanakitti S, Wattanapornphan P and Srimanosawapak S 2010 Characteristics of porous alumina produced by freeze casting *J. Microsc. Soc. Thail.* **24** 126–9
- [82] Guo R, Wang C-A and Yang A 2011 Piezoelectric properties of the 1–3 type porous lead zirconate titanate ceramics *J. Am. Ceram. Soc.* **94** 1794–9
- [83] Guo R, Wang C-A and Yang A 2011 Effects of pore size and orientation on dielectric and piezoelectric properties of 1–3 type porous PZT ceramics *J. Eur. Ceram. Soc.* **31** 605–9
- [84] Ye F, Zhang J, Liu L and Zhan H 2011 Effect of solid content on pore structure and mechanical properties of porous silicon nitride ceramics produced by freeze casting *Mater. Sci. Eng. A* **528** 1421–4
- [85] Liu X, Rahaman M N and Fu Q 2011 Oriented bioactive glass (13–93) scaffolds with controllable pore size by unidirectional freezing of camphene-based suspensions: microstructure and mechanical response *Acta Biomater.* **7** 406–16
- [86] Zhao K, Tang Y-F, Qin Y-S and Wei J-Q 2011 Porous hydroxyapatite ceramics by ice templating: freezing characteristics and mechanical properties *Ceram. Int.* **37** 635–9
- [87] Ye F, Zhang J, Zhang H and Liu L 2010 Pore structure and mechanical properties in freeze cast porous  $Si_3N_4$  composites using polyacrylamide as an addition agent *J. Alloys Compd* **506** 423–7
- [88] Ye F, Zhang J, Zhang H and Liu L 2010 Effect of sintering temperature on microstructure and mechanical properties of highly porous silicon nitride ceramics produced by freeze casting *Mater. Sci. Eng. A* **527** 6501–4
- [89] Nakata M, Fukushima M and Yoshizawa Y-I 2007 *Advanced Processing and Manufacturing Technologies for Structural and Multifunctional Materials* ed T Ohji et al (Hoboken, NJ: Wiley)
- [90] Ding S, Zeng Y-P and Jiang D 2007 Fabrication of mullite ceramics with ultrahigh porosity by gel freeze drying *J. Am. Ceram. Soc.* **90** 2276–9
- [91] Landi E, Valentini F and Tampieri A 2008 Porous hydroxyapatite/gelatine scaffolds with ice-designed channel-like porosity for biomedical applications *Acta Biomater.* **4** 1620–6
- [92] Fife J, Li J, Dunand D C and Voorhees P 2011 Morphological analysis of pores in directionally freeze-cast titanium foams *J. Mater. Res.* **24** 117–24
- [93] Jung H-D, Yook S-W, Kim H-E and Koh Y-H 2009 Fabrication of titanium scaffolds with porosity and pore size

- gradients by sequential freeze casting *Mater. Lett.* **63** 1545–7
- [94] Chino Y and Dunand D C 2008 Directionally freeze-cast titanium foam with aligned, elongated pores *Acta Mater.* **56** 105–13
- [95] Fu Q, Rahaman M N, Dogan F and Bal B S 2008 Freeze casting of porous hydroxyapatite scaffolds: II. Sintering, microstructure, and mechanical behavior *J. Biomed. Mater. Res. B: Appl. Biomater.* **86** 514–22
- [96] Fu Q, Rahaman M N, Dogan F and Bal B S 2008 Freeze-cast hydroxyapatite scaffolds for bone tissue engineering applications *Biomed. Mater.* **3** 025005
- [97] Fu Q, Rahaman M N, Dogan F and Bal B S 2008 Freeze casting of porous hydroxyapatite scaffolds: I. Processing and general microstructure *J. Biomed. Mater. Res. B: Appl. Biomater.* **86** 125–35
- [98] Deville S, Saiz E and Tomsia A P 2006 Freeze casting of hydroxyapatite scaffolds for bone tissue engineering *Biomaterials* **27** 5480–9
- [99] Deng Z-Y, Fernandes H R, Ventura J M, Kannan S and Ferreira J M F 2007 Nano-TiO<sub>2</sub>-coated unidirectional porous glass structure prepared by freeze drying and solution infiltration *J. Am. Ceram. Soc.* **90** 1265–8
- [100] Cao Y and He J 2009 Preparation and formation mechanism of porous ultralightweight zirconia by ice templating *Chin. J. Mater. Res.* **23** 518–23
- [101] Bettge M, Niculescu H and Gielisse P 2004 Engineered porous ceramics using a directional freeze-drying process *27th Int. Spring Seminar Electronics Technology: IEEE Meeting the Challenges of Electronics Technology Progress (2005)* pp 28–34
- [102] Araki K and Halloran J W 2005 Porous ceramic bodies with interconnected pore channels by a novel freeze casting technique *J. Am. Ceram. Soc.* **88** 1108–14
- [103] Zuo K-H, Zeng Y-P and Jiang D 2008 Properties of microstructure-controllable porous yttria-stabilized zirconia ceramics fabricated by freeze casting *Int. J. Appl. Ceram. Technol.* **5** 198–203
- [104] Zhang Y, Hu L, Han J and Jiang Z 2010 Freeze casting of aqueous alumina slurries with glycerol for porous ceramics *Ceram. Int.* **36** 617–21
- [105] Yoon B-H, Choi W-Y, Kim H, Kim J and Koh Y 2008 Aligned porous alumina ceramics with high compressive strengths for bone tissue engineering *Scr. Mater.* **58** 537–40
- [106] Yoon B-H, Park C-S, Kim H-E and Koh Y-H 2007 *In situ* synthesis of porous silicon carbide (SiC) ceramics decorated with SiC nanowires *J. Am. Ceram. Soc.* **90** 3759–66
- [107] Yoon B-H, Koh Y-H, Park C-S and Kim H-E 2007 Generation of large pore channels for bone tissue engineering using camphene-based freeze casting *J. Am. Ceram. Soc.* **90** 1744–52
- [108] Yook S-W, Kim H-E and Koh Y-H 2009 Fabrication of porous titanium scaffolds with high compressive strength using camphene-based freeze casting *Mater. Lett.* **63** 1502–4
- [109] Yook S-W, Kim H-E, Yoon B-H, Soon Y-M and Koh Y-H 2009 Improvement of compressive strength of porous hydroxyapatite scaffolds by adding polystyrene to camphene-based slurries *Mater. Lett.* **63** 955–8
- [110] Yang T, Ji H, Yoon S, Kim B and Park H 2010 Porous mullite composite with controlled pore structure processed using a freeze casting of TBA-based coal fly ash slurries *Resour. Conserv. Recycl.* **54** 816–20
- [111] Tang Y, Zhao K, Wei J-Q and Qin Y 2010 Fabrication of aligned lamellar porous alumina using directional solidification of aqueous slurries with an applied electrostatic field *J. Eur. Ceram. Soc.* **30** 1963–5
- [112] Tallón C, Moreno R and Nieto I M 2009 Shaping of porous alumina bodies by freeze casting *Adv. Appl. Ceram.* **108** 307–13
- [113] Suetsugu Y, Hotta Y, Iwasashi M, Sakane M, Kikuchi M, Ikoma T, Higaki T, Ochiai N and Tanaka J 2007 Structural and tissue reaction properties of novel hydroxyapatite ceramics with unidirectional pores *Key Eng. Mater.* **330–332** 1003–6
- [114] Song J-H, Koh Y-H, Kim H-E, Li L-H and Bahn H-J 2006 Fabrication of a porous bioactive glass–ceramic using room-temperature freeze casting *J. Am. Ceram. Soc.* **89** 2649–53
- [115] Soon Y-M, Shin K-H, Koh Y-H, Lee J-H and Kim H-E 2009 Compressive strength and processing of camphene-based freeze cast calcium phosphate scaffolds with aligned pores *Mater. Lett.* **63** 1548–50
- [116] Moon J-W, Hwang H-J, Awano M and Maeda K 2003 Preparation of NiO/YSZ tubular support with radially aligned pore channels *Mater. Lett.* **57** 1428–34
- [117] Mallick K K 2009 Freeze casting of porous bioactive glass and bioceramics *J. Am. Ceram. Soc.* **92** S85–94
- [118] Macchetta A, Turner I G and Bowen C R 2009 Fabrication of HA/TCP scaffolds with a graded and porous structure using a camphene-based freeze-casting method *Acta Biomater.* **5** 1319–27
- [119] Liu G, Zhang D, Meggs C and Button T W 2010 Porous Al<sub>2</sub>O<sub>3</sub>–ZrO<sub>2</sub> composites fabricated by an ice template method *Scr. Mater.* **62** 466–8
- [120] Lee E-J, Koh Y-H, Yoon B-H, Kim H-E and Kim H-W 2007 Highly porous hydroxyapatite bioceramics with interconnected pore channels using camphene-based freeze casting *Mater. Lett.* **61** 2270–3
- [121] Lee S-H, Jun S-H, Kim H-E and Koh Y-H 2008 Piezoelectric properties of PZT-based ceramic with highly aligned pores *J. Am. Ceram. Soc.* **91** 1912–5
- [122] Lee S-H, Jun S-H, Kim H-E and Koh Y-H 2007 Fabrication of porous PZT-PZN piezoelectric ceramics with high hydrostatic figure of merits using camphene-based freeze casting *J. Am. Ceram. Soc.* **90** 2807–13
- [123] Koh Y-H, Sun J-J and Kim H-E 2007 Freeze casting of porous Ni–YSZ cermets *Mater. Lett.* **61** 1283–7
- [124] Ji H B, Kim W Y, Yang T-Y, Yoon S Y, Kim B K and Park H C 2010 Freeze casting of aqueous coal fly ash/ alumina slurries for preparation of porous ceramics *J. Phys. Chem. Solids* **71** 503–6
- [125] Hong C, Zhang X, Han J, Du J and Zhang W 2010 Camphene-based freeze-cast ZrO<sub>2</sub> foam with high compressive strength *Mater. Chem. Phys.* **119** 359–62
- [126] Hong C, Zhang X, Han J, Du J and Han W 2009 Ultra-high-porosity zirconia ceramics fabricated by novel room-temperature freeze-casting *Scr. Mater.* **60** 563–6
- [127] Han J, Hong C, Zhang X, Du J and Zhang W 2010 Highly porous ZrO<sub>2</sub> ceramics fabricated by a camphene-based freeze-casting route: microstructure and properties *J. Eur. Ceram. Soc.* **30** 53–60
- [128] Fukasawa T, Deng Z-Y, Ando M, Ohji T and Kanzaki S 2002 Synthesis of porous silicon nitride with unidirectionally aligned channels using freeze-drying process *J. Am. Ceram. Soc.* **85** 2151–5
- [129] Fukushima M, Nakata M and Yoshizawa Y-I 2008 Fabrication and properties of ultra highly porous cordierite with oriented micrometer-sized cylindrical pores by gelation and freezing method *J. Ceram. Soc. Japan* **116** 1322–5
- [130] Fukushima M, Nakata M, Zhou Y, Ohji T and Yoshizawa Y-I 2010 Fabrication and properties of ultra highly porous silicon carbide by the gelation–freezing method *J. Eur. Ceram. Soc.* **30** 2889–96
- [131] Fukasawa T, Ando M, Ohji T and Kanzaki S 2001 Synthesis of porous ceramics with complex pore structure by freeze-dry processing *J. Am. Ceram. Soc.* **84** 230–2

- [132] Fu Q, Rahaman M N, Bal B S and Brown R F 2010 Preparation and *in vitro* evaluation of bioactive glass (13–93) scaffolds with oriented microstructures for repair and regeneration of load-bearing bones *J. Biomed. Mater. Res. A* **93** 1380–90
- [133] Wildhack S and Aldinger F 2006 Freeze casting of aluminium nitride *Adv. Sci. Technol.* **45** 407–12
- [134] Deville S, Saiz E, Nalla R K and Tomsia A P 2006 Freezing as a path to build complex composites *Science* **311** 515–8
- [135] Flauder S, Sajzew R and Müller F A 2015 Mechanical properties of porous  $\beta$ -tricalcium phosphate composites prepared by ice-templating and poly( $\epsilon$ -caprolactone) Impregnation *ACS Appl. Mater. Interfaces* **7** 845–51
- [136] Sepúlveda R, Plunk A A and Dunand D C 2015 Microstructure of  $\text{Fe}_2\text{O}_3$  scaffolds created by freeze-casting and sintering *Mater. Lett.* **142** 56–9
- [137] Liu R, Zhang F, Su W, Zhao H and Wang C-A 2015 Impregnation of porous mullite with  $\text{Na}_2\text{SO}_4$  phase change material for thermal energy storage *Sol. Energy Mater. Sol. Cells* **134** 268–74
- [138] Fukasawa T, Ando M and Ohji T 2002 Filtering properties of porous ceramics with unidirectionally aligned pores *J. Ceram. Soc. Japan* **110** 627–31
- [139] Fukushima M and Yoshizawa Y-I 2014 Fabrication of highly porous silica thermal insulators prepared by gelation-freezing route *J. Am. Ceram. Soc.* **93** 713–7
- [140] Pekor C M, Groth B and Nettleship I 2010 The effect of polyvinyl alcohol on the microstructure and permeability of freeze-cast alumina *J. Am. Ceram. Soc.* **93** 115–20
- [141] Zuo K-H, Zeng Y-P and Jiang D 2010 Effect of polyvinyl alcohol additive on the pore structure and morphology of the freeze-cast hydroxyapatite ceramics *Mater. Sci. Eng. C* **30** 283–7
- [142] Yoon B-H 2008 *In situ* fabrication of porous hydroxyapatite (HA) scaffolds with dense shells by freezing HA/camphene slurry *Mater. Lett.* **62** 1700–3
- [143] Zeng J, Zhang Y, Zhou K-C and Zhang D 2014 Effects of alcohol additives on pore structure and morphology of freeze-cast ceramics *Trans. Nonferr. Met. Soc. China* **24** 718–22
- [144] Perez F and Granger B E 2007 IPython: a system for interactive scientific computing *Comput. Sci. Eng.* **9** 21–9
- [145] Deville S, Maire E, Lasalle A, Bogner A, Gauthier C, Leloup J and Guizard C 2009 *In situ* x-ray radiography and tomography observations of the solidification of aqueous alumina particle suspensions: I. Initial instants *J. Am. Ceram. Soc.* **92** 2489–96
- [146] Lock P A, Jing X, Zimmerman R W and Schlueter E M 2002 Predicting the permeability of sandstone from image analysis of pore structure *J. Appl. Phys.* **92** 6311
- [147] Mallick K K and Winnett J 2012 Preparation and characterization of porous bioglass® and PLLA scaffolds for tissue engineering applications *J. Am. Ceram. Soc.* **95** 2680–6
- [148] Xie X, Zhou Y, Bi H, Yin K, Wan S and Sun L 2013 Large-range control of the microstructures and properties of three-dimensional porous graphene *Sci. Rep.* **3** 2117
- [149] Sun H, Xu Z and Gao C 2013 Multifunctional, ultra-flyweight, synergistically assembled carbon aerogels *Adv. Mater.* **25** 2554–60
- [150] Waschki T, Oberacker R and Hoffmann M J 2009 Control of lamellae spacing during freeze casting of ceramics using double-side cooling as a novel processing route *J. Am. Ceram. Soc.* **92** S79–84
- [151] Bareggi A, Maire E, Lasalle A and Deville S 2011 Dynamics of the freezing front during the solidification of a colloidal alumina aqueous suspension: *in situ* x-ray radiography, tomography, and modeling *J. Am. Ceram. Soc.* **94** 3570–8
- [152] Scheffler M and Colombo P 2005 *Cellular Ceramics: Structure, Manufacturing, Properties and Applications* (New York: Wiley)
- [153] Ashby M F and Medalist R F M 1983 The mechanical properties of cellular solids *Metall. Trans. A* **14** 1755–69
- [154] Studart A R, Gonzenbach U T, Tervoort E and Gauckler L J 2006 Processing routes to macroporous ceramics: a review *J. Am. Ceram. Soc.* **89** 1771–89
- [155] Meille S, Lombardi M, Chevalier J and Montanaro L 2012 Mechanical properties of porous ceramics in compression: on the transition between elastic, brittle, and cellular behavior *J. Eur. Ceram. Soc.* **32** 3959–67
- [156] Lasalle A, Guizard C, Maire E, Adrien J and Deville S 2012 Particle redistribution and structural defect development during ice templating *Acta Mater.* **60** 4594–603
- [157] Style R W and Peppin S S 2012 The kinetics of ice-lens growth in porous media *J. Fluid Mech.* **692** 482–98
- [158] Peppin S S, Majumdar A, Style R W and Sander G 2011 Frost heave in colloidal soils *SIAM J. Appl. Math.* **71** 1717
- [159] Anderson A M and Grae Worster M 2014 Freezing colloidal suspensions: periodic ice lenses and compaction *J. Fluid Mech.* **758** 786–808
- [160] Style R W, Peppin S S, Cocks A and Wettlaufer J S 2011 Ice-lens formation and geometrical supercooling in soils and other colloidal materials *Phys. Rev. E* **84** 1–12
- [161] Chantikul P 1990 Role of grain size in the strength and R-curve properties of alumina *J. Am. Ceram. Soc.* **73** 2419–27
- [162] Hu L, Wang C-A, Huang Y, Sun C, Lu S and Hu Z 2010 Control of pore channel size during freeze casting of porous YSZ ceramics with unidirectionally aligned channels using different freezing temperatures *J. Eur. Ceram. Soc.* **30** 3389–96
- [163] Münch E, Saiz E, Tomsia A P and Deville S 2009 Architectural control of freeze-cast ceramics through additives and templating *J. Am. Ceram. Soc.* **92** 1534–9
- [164] Gibson L J 2005 Biomechanics of cellular solids *J. Biomech.* **38** 377–99
- [165] Zhang J and Ashby M F 1992 The out-of-plane properties of honeycombs *Int. J. Mech. Sci.* **34** 475–89
- [166] Liu X, Rahaman M N, Fu Q and Tomsia A P 2012 Porous and strong bioactive glass (13–93) scaffolds prepared by unidirectional freezing of camphene-based suspensions *Acta Biomater.* **8** 415–23
- [167] Deville S, Viuzzi C, Leloup J, Lasalle A, Guizard C, Maire E, Adrien J and Gremillard L 2011 Ice shaping properties, similar to that of antifreeze proteins, of a zirconium acetate complex *PLoS One* **6**e26474
- [168] Porter M M, Imperio R, Wen M, Meyers M A and McKittrick J 2014 Bioinspired scaffolds with varying pore architectures and mechanical properties *Adv. Funct. Mater.* **24** 1978–87
- [169] Riblett B W, Francis N L, Wheatley M A and Wegst U G K 2012 Ice-templated scaffolds with microridged pores direct drug neurite growth *Adv. Funct. Mater.* **22** 4920–3
- [170] Ojuva A, Järveläinen M, Bauer M, Keskinen L, Valkonen M, Akhtar F, Levänen E and Bergström L 2015 Mechanical performance and  $\text{CO}_2$  uptake of ion-exchanged zeolite structured by freeze-casting *J. Eur. Ceram. Soc.* **35** 2607–18
- [171] Petit C, Meille S and Maire E 2013 Cellular solids studied by x-ray tomography and finite element modeling—a review *J. Mater. Res.* **28** 2191–201
- [172] Liu X, Martin C L, Delette G and Bouvard D 2010 Elasticity and strength of partially sintered ceramics *J. Mech. Phys. Solids* **58** 829–4